Understanding cavity resonances with intracavity dispersion properties

Jiteng Sheng, Haibin Wu, M. Mumba, J. Gea-Banacloche, and Min Xiao

Phys. Rev. A **83**, 023829 — Published 28 February 2011

DOI: 10.1103/PhysRevA.83.023829

Understanding cavity resonances with intracavity dispersion properties

Jiteng Sheng, Haibin Wu, M. Mumba, J. Gea-Banacloche, and Min Xiao

Department of Physics, University of Arkansas, Fayetteville AR 72701, USA

We experimentally study the strongly-coupled three-level atom-cavity system at both cavity and coupling frequency detuning cases. Side peak splitting and anti-crossing-like phenomena are observed under different experimental conditions. Intracavity dispersion properties are used to explain qualitatively the complicated cavity resonance structures in the composite system of inhomogeneously-broadened three-level atoms inside an optical ring cavity with relatively strong driving intensities.

PACS number(s) 42.50.Pq, 32.80.-t, 42.50.Gy

I. INTRODUCTION

Coupled atom-cavity systems under strong coupling condition, which are typically classified as cavity quantum electrodynamics (cavity-QED), have been of great interest in recent years [1-3]. Many experiments have been performed in strongly coupled two-level atom-cavity systems, in which the "normal-mode splitting" (or Rabi splitting) phenomenon has been observed [4-15]. When three-level coherently-prepared (or electromagnetically induced transparency (EIT) [16,17]) atoms are placed inside an optical cavity, a third polariton branch (i.e. dark-polariton [18]) appears in the middle of the cavity transmission spectrum. Recently, coupled three-level atom-cavity systems have been experimentally investigated with cold atoms [19], hot atomic vapor [20], and a single atom [21].

In investigating simple systems, such as cavity coupled with homogeneously-broadened two-level atoms [4] or with three-level atoms on resonance [20], it is possible to explain the cavity transmission peak structures by solving Maxwell-Bloch or density-matrix equations. When fully considering the transmission spectrum of an atom-cavity system coupled with three-level Doppler-broadened atoms (including frequency detunings), we show here that by combining the atomic dispersion properties [5] with the round-trip phase for the intracavity medium, the complicated cavity transmission spectra can be well explained under different experimental conditions. The linear/nonlinear intracavity dispersion properties give a good physical picture to understand the complicated peak structures in the cavity transmission spectra from such

coupled three-level atom-cavity system, even with cavity，and coupling field frequency detunings.

II. THEORETICAL CONSIDERATIONS

We will mainly use the linear dispersion property to first qualitatively explain the cavity transmission, and then include the nonlinear dispersion contribution in fitting the experimental data. The advantage of only considering the linear dispersion is that it is sufficient to understand the main features of the cavity transmission peaks (such as the number of peaks and their positions). The nonlinear effect only changes the shapes of the cavity transmission peaks and slightly modifies their positions, when the nonlinearity is not very strong.

The linear complex susceptibility of the three-level Doppler-broadened EIT atoms is given by [17]

$$\chi = \frac{4i\hbar c g_{12}^2 N_0 \sqrt{\pi}}{\varepsilon_0 u \omega_p} e^{z^2} (1 - erfz) \tag{1}$$

with the argument

$$z = \frac{c}{u\omega_p}(\gamma_{21} - i\Delta_p + \frac{\Omega_c^2 / 4}{\gamma_{31} - i(\Delta_p - \Delta_c)}), \tag{2}$$

where $\Delta_p = \omega_p - \omega_{12}$ is the probe frequency detuning and $\Delta_c = \omega_c - \omega_{32}$ is the coupling frequency detuning; Ω_c is the Rabi frequency of the coupling field; $u/\sqrt{2}$ is the root-mean-square atomic velocity. The decay rates are given by $\gamma_{ij} = (\Gamma_i + \Gamma_j)/2$, where

Γ_i is the natural decay rate of the energy level |i>.

In general, the intensity transmission function of the coupled atom-cavity system is given by (see Ref. [5])

$$S(\omega_p) = \frac{T^2}{1 + R^2\kappa^2 - 2R\kappa\cos[(\Delta + (\omega_p \mathrm{l}/2\mathrm{L})\chi')\mathrm{L}/\mathrm{c}]}, \tag{3}$$

where T and R are the transmissivity and the reflectivity of the mirrors, respectively, and $\kappa \equiv \exp[-\omega_p l \chi''/c]$ describes the intracavity absorption. $\chi = \chi' + i\chi''$ with χ' being the dispersion and χ'' the absorption components. $\Delta = \Delta_p - \Delta_\theta$ describes the total frequency detuning, where $\Delta_\theta = \omega_{cav} - \omega_{12}$ is the cavity frequency detuning. If the coupling and cavity frequency detunings are both zero, the system is said to be on resonance [22]. When $\Delta + (\omega_p l/2L)\chi'$ equals to zero, the intensity transmission function $S(\omega_p)$ has its maximum value, which corresponds to a peak in the cavity transmission spectrum. We define the detuning line as $-\Delta$, and the modified dispersion curve as $(\omega_p l/2L)\chi'$ in plotting Eq. (3). When these two curves have an intersection, there is a peak in the transmission (transmission intensity vs probe frequency detuning). Even when the detuning line $(-\Delta)$ and the modified dispersion curve $((\omega_p l/2L)\chi')$ don't have intersections, the places, where the absolute difference between the detuning line $(-\Delta)$ and the dispersion curve $((\omega_p l/2L)\chi')$ has the minimum value, could still generate transmission peaks (e.g. maximum values in Eq. (3) in the transmission).

First, let's consider two on-resonance ($\Delta_\theta = \Delta_c = 0$) cases [20,22], as shown in Fig. 1. One could observe three cavity transmission peaks in both cases as shown in Figs. 1(c)

and 1(d), respectively. In case (a), the detuning line ($-\Delta = -\Delta_p$) does not cross the dispersion curve ($(\omega_p l/2L)\chi'$) except at $\Delta_p = 0$, however, there still exist two broader side peaks at points where the difference between the dispersion curve ($(\omega_p l/2L)\chi'$) and the detuning line ($-\Delta = -\Delta_p$) is minimum (Fig. 1(c)). In case (b), the detuning line ($-\Delta = -\Delta_p$) crosses the dispersion curve ($(\omega_p l/2L)\chi'$) at several places. Since there are five crossings, one could expect to observe five peaks under certain experimental conditions [22]. However, since the absorption is large near the resonance as shown by the dotted curve in Fig. 1(b), at a relatively low probe intensity, the two peaks close to the probe resonance are severely absorbed (barely seen) leaving a three-peak structure (Fig. 1(d)) with two narrower side peaks.

Now, we can explain the cavity transmission spectrum when the cavity is detuned from its resonance using the dispersion picture. Figure 2 depicts the cavity detuning case for the situation shown in Fig. 1(a). The calculated dispersion function $(\omega_p l/2L)\chi'$ is plotted as a solid red curve. The green dashed lines give the detuning line $-\Delta = -(\Delta_p - \Delta_\theta)$ at different cavity detunings. The left dashed green line (i) is for the on-resonance case ($\Delta_\theta = \Delta_c = 0$), which shows three symmetric peaks in the cavity transmission (Fig. 1(c)); the middle dashed green line (ii) and the right dashed green line (iii) are for the cases with cavity detunings ($\Delta_\theta \neq 0, \Delta_c = 0$), which lead to the complicated, asymmetric cavity transmission spectra. Before going into such complicated cavity transmission cases, we will present our experimental observations.

III. EXPERIMENTAL OBSERVATIONS

The experimental setup is shown in Fig. 3. A three-mirror optical ring cavity is composed of an input mirror M1 and an output mirror M2 with 3% and 1.4% transmissivities, respectively; and a high reflector M3 mounted on a PZT for cavity frequency scanning and locking. The cavity length L=37 cm. The rubidium vapor cell is 5 cm long with Brewster windows, and is wrapped in μ-metal sheets for magnetic field shielding and in heat tape for heating. Three energy levels in D1 line of ^{87}Rb atoms are used for the three-level Λ-type EIT system [20]. The coupling beam is injected through a polarization beam splitter (PBS), which does not circulate in the cavity. The probe beam is injected into the cavity via the input mirror M1 and circulates in the cavity as the cavity field, and the output is detected by an avalanche photo-diode detector (APD). The radii of the coupling and probe beams are estimated to be 600 μm and 100 μm at the center of the atomic cell, respectively. The empty cavity finesse is about 100. When the atomic cell and PBS are included, the cavity finesse decreases to about 48.

Figure 4 plots the experimentally measured and theoretically calculated positions of the cavity transmission peaks versus the probe frequency detuning (Δ_p) for different cavity detuning (Δ_θ) values. One can see the similar transmission spectrum as reported in Ref. [20] (at a slightly higher temperature of T=80.3 ºC) in Fig. 4(d1), at the resonant case ($\Delta_\theta = \Delta_c = 0$), with symmetric side peaks. When the cavity is positively detuned to around 20 MHz, the right side peak begins to split into two peaks (Fig. 4(c1)). As the

cavity detuning (Δ_θ) further increases, one of the split peaks moves outwards and another moves inwards (Fig. 4(b1)). When $\Delta_\theta \approx 160$ MHz, as shown in Fig. 4(a1), the inward-moving peak merges with the central peak. If the cavity is negatively detuned, one can see a similar behavior for the left side peak (Figs. 4(e1)-(g1)).

The central peak positions in Figs. 4(a1)-(g1) have slight changes, as shown in the inset of Fig. 5. The position of the central peak is determined by the frequency-pulling equation [23]:

$$\omega_r = \frac{1}{1+\eta}\omega_{cav} + \frac{\eta}{1+\eta}\omega_{12}. \tag{4}$$

Here, $\eta = \frac{\omega_p l}{2L}\frac{\partial \chi'}{\partial \Delta_p}$ defines the frequency-locking coefficient. This is quite different from the result presented in Ref. [19], in which the cavity detuning Δ_θ could not get too large since the atomic density in that experiment is relatively low, and the dispersion slope around the EIT resonance is too sharp ($\eta = \frac{\omega_p l}{2L}\frac{\partial \chi'}{\partial \Delta_p} \approx 25$) to observe the frequency shift of the central peak due to the frequency pulling effect. In the current experimental system, the dispersion slope around the center (near resonance) is not that sharp and the cavity can be detuned as far as 250 MHz, so it is possible to observe the frequency shift of the central peak position (frequency pulling) beyond noise range as predicted by Eq. (4). By measuring the slope in the inset of Fig. 5, one can roughly calculate the group index and the group velocity. Looking at the dispersion curve in Fig. 2, we would get the same solution as in Fig. 2. The left dashed green line (i) in Fig. 2 gives the resonant case

for the cavity, which corresponds to the case in Fig. 4(d1); the middle dashed green line (ii) in Fig. 2 corresponds to the splitting of the right side peak, which is the case in Fig. 4(c1); and the right dashed green line (iii) in Fig. 2 gives the case where the central peak and one of the split peaks begin to merge, which corresponds to Fig. 4(a1). We can choose ω_{12} as the origin (i.e. zero detuning) and rewrite Eq. (4) as $\Delta_r = \frac{1}{1+\eta}\Delta_\theta$ with $\Delta_r = \omega_r - \omega_{12}$. From the inset of Fig. 5, the slope can be determined to be $\Delta_r / \Delta_\theta \approx 0.1$, which gives $\eta = \frac{\omega_p l}{2L}\frac{\partial \chi'}{\partial \Delta_p} \approx 9$ in the current case. The group index of the intracavity dispersive medium can be written as $n_g \approx n + \omega_p \frac{1}{2}\frac{\partial \chi'}{\partial \omega_p}$, which gives $n_g \approx 68$ under the current experimental condition.

Figures 4(a2)-(g2) present the results of the numerical calculations based on full nonlinear theory. In this calculation, unlike in our previous publications, no plane-wave approximation is made for the probe beam (cavity field) although the coupling beam is still assumed to be a plane wave. The paraxial wave propagation equation is integrated numerically with the calculated nonlinear susceptibility for a number of cavity roundtrips, starting from a zero cavity field until it converges into a steady state. As one can see that the basic features of the experimentally observed spectra showing in Figs. 4(a1)-(g1) can be found in the corresponding theoretically stimulated curves (Figs. 4(a2)-(g2)). However, in spite of the relative sophistication of this calculation, the agreement with the experimental data is still only qualitative, suggesting that more work

still needs to be done on the modeling of this coupled nonlinear system.

Next, we consider the second cavity detuning case shown in Fig. 1(b). When the detuning line is moved parallel to itself, the positions of the side peaks also move, leading to an anti-crossing-like curve. Figure 6(a) shows the experimentally measured transmission spectrum at the cavity detuning of $\Delta_0 \approx$-200 MHz, and Fig. 6(b) plots the positions of the three peaks as a function of the cavity detuning, which exhibits an anti-crossing-like behavior for the two side (the "bright polariton") peaks. One can easily explain such anti-crossing behavior as in the coupled two-level atom-cavity systems [8]. One of the main differences between this coupled three-level atom-cavity system and the two-level atom-cavity system is that in such three-level system, there will always be gaps between the central peak and the two side peaks, which depend on the shape of the dispersion curve.

Now, we examine the case with coupling frequency detuning. When the coupling detuning is very small, the dispersion curve is slightly shifted in the horizontal direction while the detuning line still passes through the origin. This actually is quite similar to the cavity frequency detuning case, where the dispersion curve is fixed with a moving detuning line. Of course, when the coupling detuning becomes large, the shape of the dispersion curve will significantly change. However, one can qualitatively understand the cavity transmission spectrum even under such conditions. Figure 7 gives the case for a homogeneously-broadened medium. Since in the homogeneously-broadened case, the value of $|\chi|$ is about 2 orders of magnitude larger than in the

inhomogeneously-broadened case, a lower atomic density can be used to simulate the system. Figure 7(a) plots the on-resonance case with Δ_0=0 and Δ_c=0, and Fig. 7(b) shows the coupling detuning case with Δ_0=0 and Δ_c=115 MHz. Although there are five crossing points for the dispersion curve with the detuning line (Fig. 7(a)), two of them are always close to the high-absorption positions. So, as in Fig. 7(c) only three peaks survive. In Fig. 7(b), the cavity is detuned to the right peak position and the dispersion curve is significantly distorted, but one still finds only three peaks in the transmission spectrum (Fig. 7(d)) (two of the five peaks are absorbed), which corresponds to the situation as described in Ref. [24].

Figure 8 presents the experimental results in the inhomogeneously-broadened three-level atomic system. Figure 8(a) depicts the cavity transmission spectrum at the coupling detuning of Δ_c=-75 MHz, and Fig. 8(b) presents the positions of the three peaks as a function of the coupling detuning. Again, one can see the anti-crossing-like behavior for the two side peaks. The center ("dark polariton") peak position changes quasi-linearly with the coupling detuning.

IV. CONCLUSION

We presented our experimental investigations of the cavity transmission spectra with inhomogeneously-broadened three-level atoms inside an optical ring cavity with cavity and coupling frequency detunings. The complicated cavity transmission peak structures can be qualitatively understood by plotting the linear dispersion curves together with the

detuning lines. The observed three-peak cavity transmission structures and their positions can be well explained by the crossing points between the dispersion curves of the intracavity medium and the detuning line. The near-resonance absorption peaks significantly affect the cavity transmission spectra and need to be considered in identifying the cavity transmission peaks. This study helps us to better understand the interactions between the strongly coupled three-level atoms and the optical cavity, which can find applications in quantum information processing.

We acknowledge the funding support of the National Science Foundation through the grant PHY-0652970.

[1] *Cavity Quantum Electrodynamics*, edited by P. R. Berman (Academic, San Diego, 1994)

[2] H. J. Kimble, Phys. Scr. **T76**, 127 (1998)

[3] G. S. Agarwal, J. Mod. Opt. **45**, 449 (1998)

[4] M. G. Raizen, R. J. Thompson, R. J. Brecha, H. J. Kimble, and H. J. Carmichael, Phys. Rev. Lett. **63**, 240 (1989).

[5] Y. Zhu, D. J. Gauthier, S. E. Morin, Q. Wu, H. J. Carmichael, and T. W. Mossberg, Phys. Rev. Lett. **64**, 2499 (1990).

[6] R. J. Thompson, G. Rempe, and H. J. Kimble, Phys. Rev. Lett. **68**, 1132 (1992)

[7] J. J. Childs, K. An, M. S. Otteson, R. R. Dasari, and M. S. Feld, Phy. Rev. Lett. **77**, 2901 (1996).

[8] J. Gripp, S. L. Mielke, and L. A. Orozco, Phys. Rev. A **56**, 3262 (1997).

[9] A. Boca, R. Miller, K. M. Birnbaum, A. D. Boozer, J. McKeever, and H. J. Kimble, Phys. Rev. Lett. **93**, 233603 (2004).

[10] P. Maunz, T. Puppe, I. Schuster, N. Syassen, P. W. H. Pinkse, and G. Rempe, Phys. Rev. Lett. **94**, 033002 (2005)

[11] A. K. Tuchman, R. Long, G. Vrijsen, J. Boudet, J. Lee, and M. A. Kasevich, Phys. Rev. A **74**, 053821 (2006)

[12] F. Brennecke, T. Donner, S. Ritter, T. Bourdel, M. Köhl, and T. Esslinger, Nature **450**, 268 (2007)

[13] J. M. Fink, M. Göppl, M. Baur, R. Bianchetti, P. J. Leek, A. Blais, and A. Wallraff,

Nature **454**, 315 (2008)

[14] M. Khudaverdyan, W. Alt, T. kampschulte, S. Reick, A. Thobe, A. Widera, and D. Meschede, Phys. Rev. Lett. **103**, 123006 (2009)

[15] Y. Choi, S. Kang, S. Lim, W. Kim, J. Kim, J. Lee, and K. An, Phys. Rev. Lett. **104**, 153601 (2010)

[16] S. E. Harris, Phys. Today **50**, 36 (1997).

[17] J. Gea-Banacloche, Y. Q. Li, S. Jin, and Min Xiao, Phys. Rev. A **51**, 576 (1995).

[18] M. Fleischhauer and M. D. Lukin, Phys. Rev. Lett. **84**, 5094 (2000).

[19] G. Hernandez, J. Zhang, and Y. Zhu, Phys, Rev. A **76**, 053814 (2007).

[20] H. Wu, J. Gea-Banacloche, and M. Xiao, Phys. Rev. Lett. **100,** 173602 (2008).

[21] M. Mücke, E. Figueroa1, J.Bochmann, C. Hahn, K. Murr, S. Ritter, C. J. Villas-Boas, and G. Rempe, Nature **465**, 755 (2010)

[22] H. Wu, J. Gea-Banacloche, and M. Xiao, Phys. Rev. A **80,** 033806 (2009).

[23] M. D. Lukin, M. Fleischhauer, and M. O. Scully, Opt. Lett. **23**, 295 (1998).

[24] J. Zhang, G. Hernandez, and Y. Zhu, Opt. Express **16**, 7860 (2008).

FIGURE CAPTIONS

Fig. 1. (Color online) Theoretical plots of dispersion curves and cavity transmission spectra versus probe frequency detuning for a Doppler-broadened three-level medium. (a) and (b): red solid curves are intracavity dispersion curves; blue dotted curves give the absorption (which are suppressed [10]); and green dashed lines are the detuning lines. (c) and (d) are the cavity transmission spectra corresponding to (a) and (b), respectively. The parameters used in the calculation are: decay rate for the probe transition $\gamma_{21} = 2\pi \times 3\ MHz$, the ground-state dephasing rate $\gamma_{31} = 2\pi \times 0.1\ MHz$, $\Omega_c = 2\pi \times 32\ MHz$, the coupling detuning $\Delta_c = 0$, the cavity detuning $\Delta_\theta = 0$, and the atomic density $N = 1.5 \times 10^{10}\ cm^{-3}$ or $N = 5 \times 10^{10}\ cm^{-3}$ for (a) and (b), respectively.

Fig. 2. (Color online) Dispersion picture at different cavity frequency detuning values. (i), (ii), and (iii) give the detuning line $-\Delta_p$ at different cavity detuning values. Other parameters used in the calculation are the same as in Fig. 1(a).

Fig. 3. (Color online) Experimental setup. PBS: polarization beam splitter; M1-M3: cavity mirrors; APD: avalanche photo-diode detector; and PZT: piezoelectric transducer.

Fig. 4. (Color online) Cavity transmission spectrum for different cavity detuning values. (a1)-(g1):The experimentally measured transmission spectra. The experimental parameters are P_p=1.7 mW, P_c=13.7 mW, Δ_c=0, and T=80.3 ºC. (a1) $\Delta_\theta \approx 160$ MHz, (b1)

$\Delta_\theta \approx 140$ MHz, (c1) $\Delta_\theta \approx 20$ MHz, (d1) $\Delta_\theta \approx 0$ MHz, (e1) $\Delta_\theta \approx -40$ MHz, (f1) $\Delta_\theta \approx -120$ MHz, (g1) $\Delta_\theta \approx -160$ MHz. (a2)-(g2): The theoretically calculated results corresponding to the measured spectra shown on (a1)-(g1), respectively. (a2) $\Delta_\theta \approx 80$ MHz, (b2) $\Delta_\theta \approx 40$ MHz, (c2) $\Delta_\theta \approx 20$ MHz, (d2) $\Delta_\theta \approx 0$ MHz, (e2) $\Delta_\theta \approx -20$ MHz, (f2) $\Delta_\theta \approx -40$ MHz, (g2) $\Delta_\theta \approx -80$ MHz.

Fig. 5. (Color online) Measured cavity transmission peak positions as a function of cavity detuning. The experimental parameters are the same as in Fig. 4. Inset: the enlarged display of the center "dark polariton" peak.

Fig. 6. (Color online) (a) Measured cavity transmission spectrum with $\Delta_\theta = -200$ MHz. (b) The positions of the polariton peaks as a function of the cavity detuning. The experimental parameters are T=84.2ºC, P_p=1.2 mW, P_c=20.8 mW.

Fig. 7. (Color online) Calculated dispersion and cavity transmission curves versus the probe detuning for a three-level homogeneously-broadened medium. (a) and (b): red solid curves show the dispersion plots; blue dotted curves present the absorptions; and green dashed lines show the detuning lines. (c) and (d) are the transmission spectra corresponding to (a) and (b), respectively. The parameters used in the calculation are: $\gamma_{21} = 2\pi \times 3\ MHz$, $\gamma_{31} = 2\pi \times 0.1\ MHz$, $\Omega_c = 2\pi \times 8\ MHz$, $N = 3 \times 10^8\ cm^{-3}$, and

$\Delta_c = 0$ (or $\Delta_c = 115\ MHz$) for (a) (or (b)).

Fig. 8. (Color online) (a) Measured cavity transmission spectrum with Δ_c= -75 MHz. (b) The positions of the polariton peaks as a function of the coupling detuning. The experimental parameters are T=76.7 ^{o}C, P_p=0.5 mW, P_c=7.0 mW.

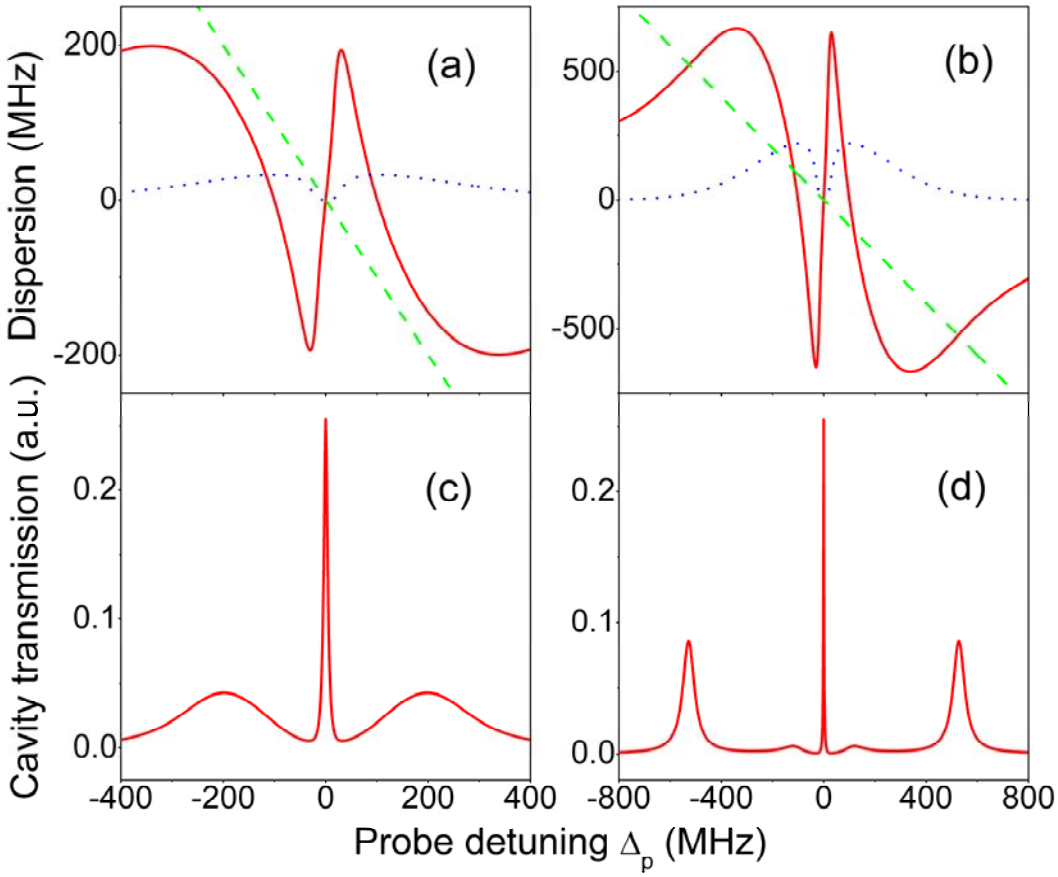

Figure 1, Sheng et al.

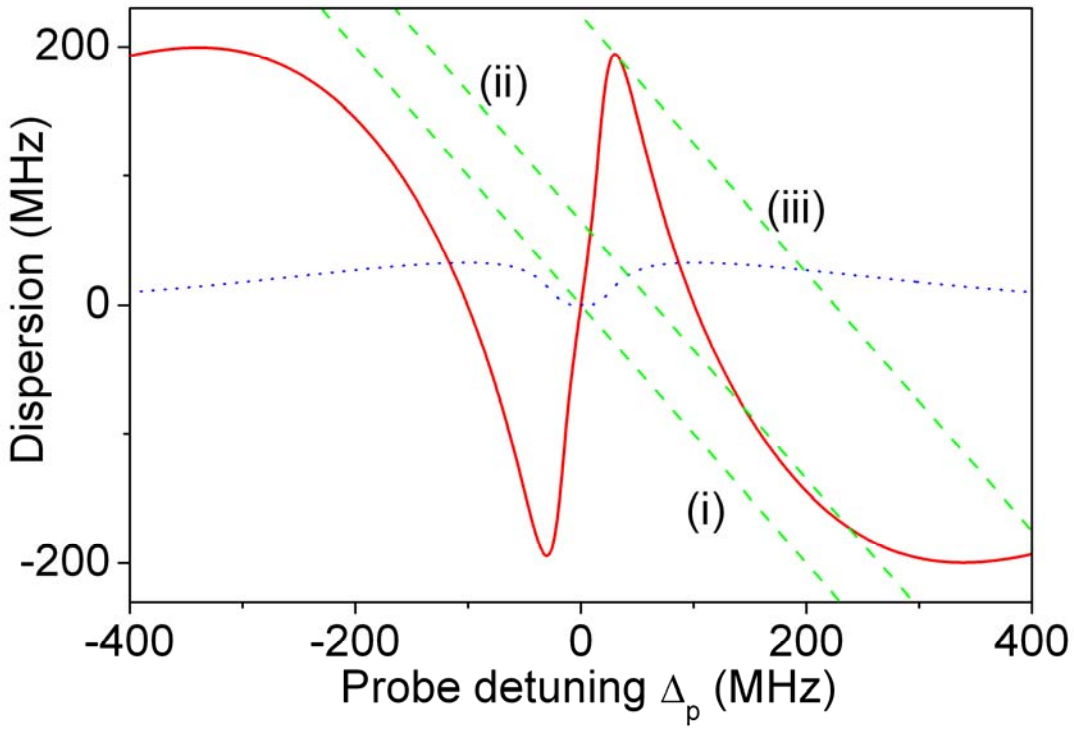

Figure 2, Sheng et al.

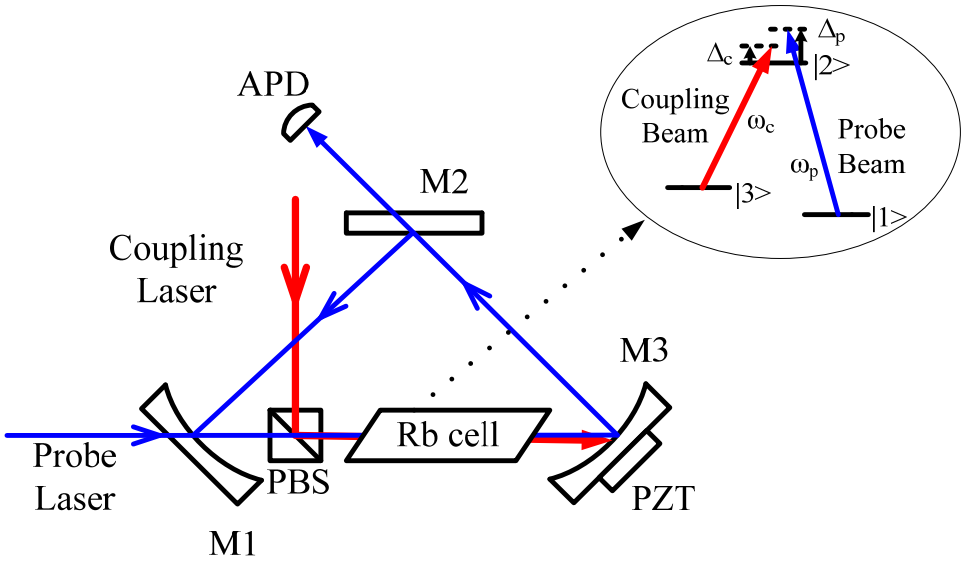

Figure 3, Sheng et al.

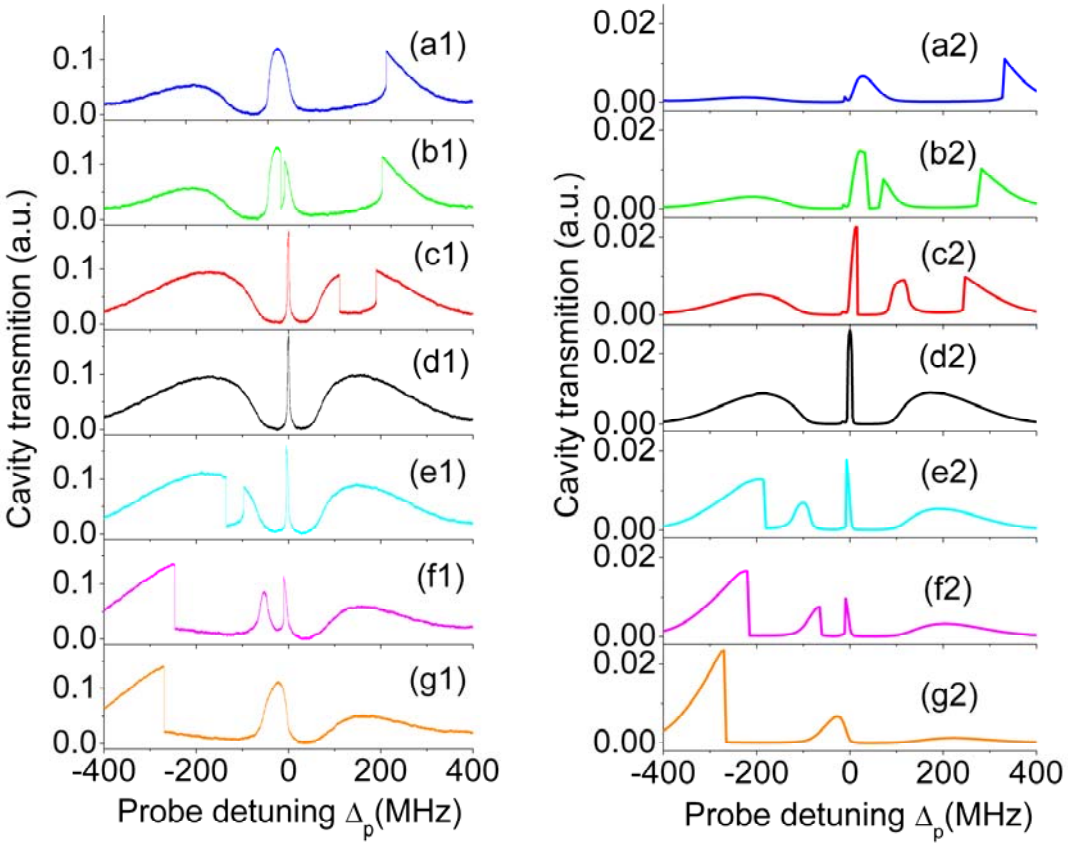

Figure 4, Sheng et al.

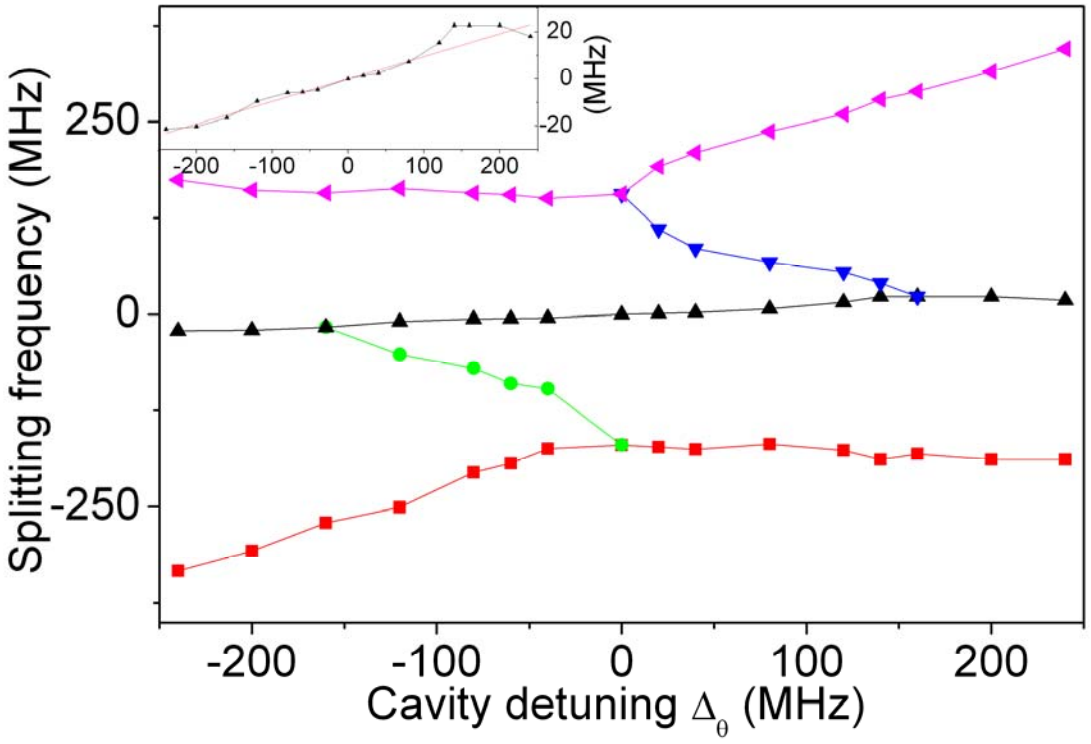

Figure 5, Sheng et al.

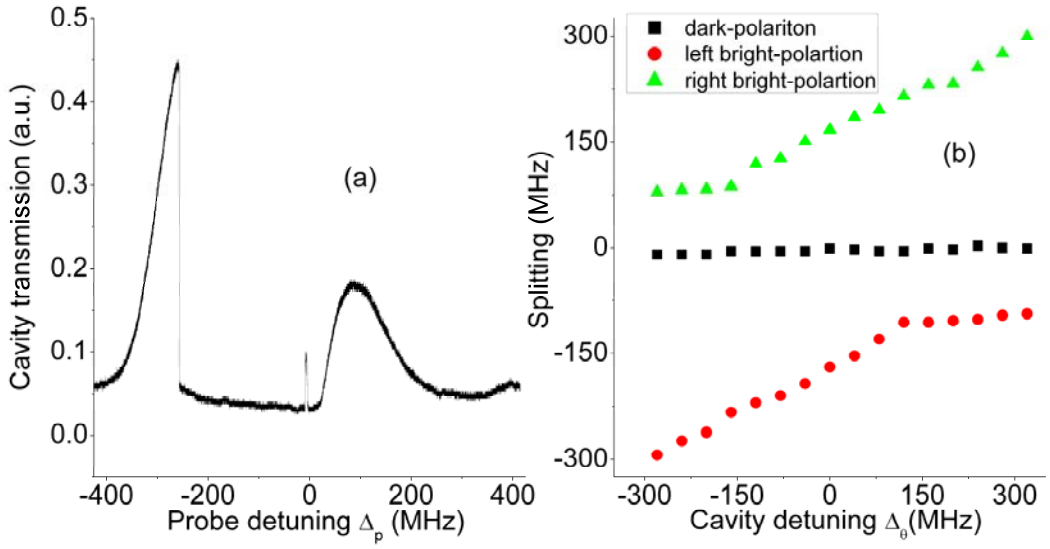

Figure 6, Sheng et al.

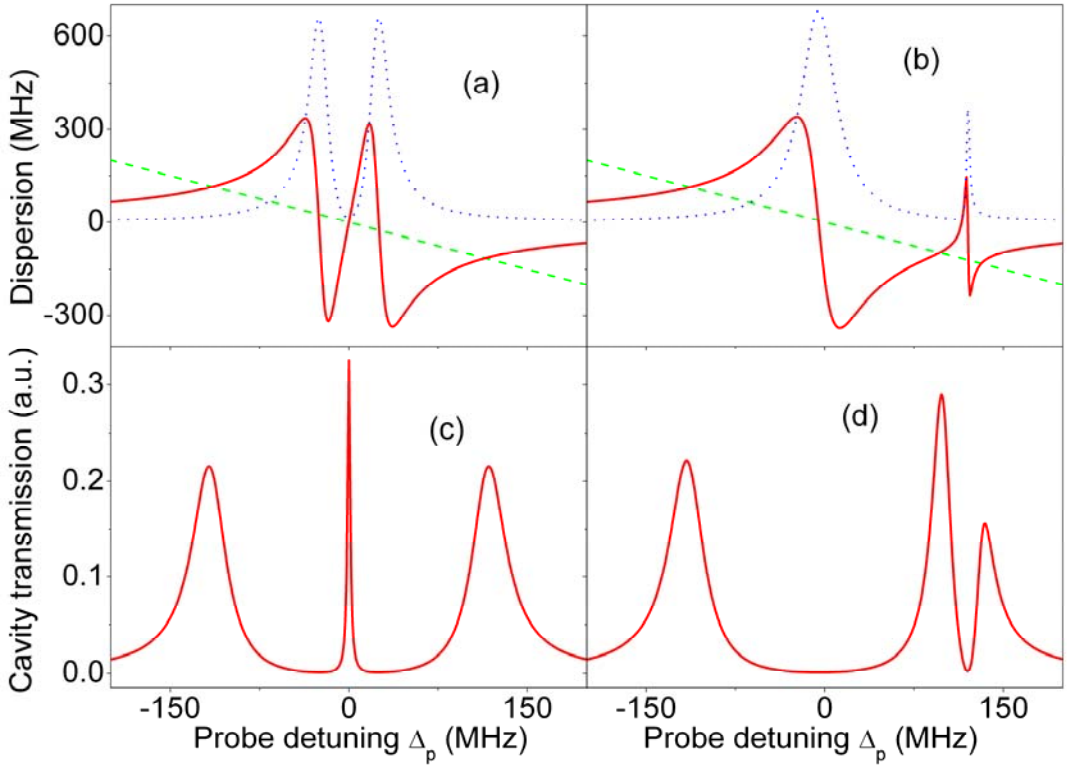

Figure 7, Sheng et al.

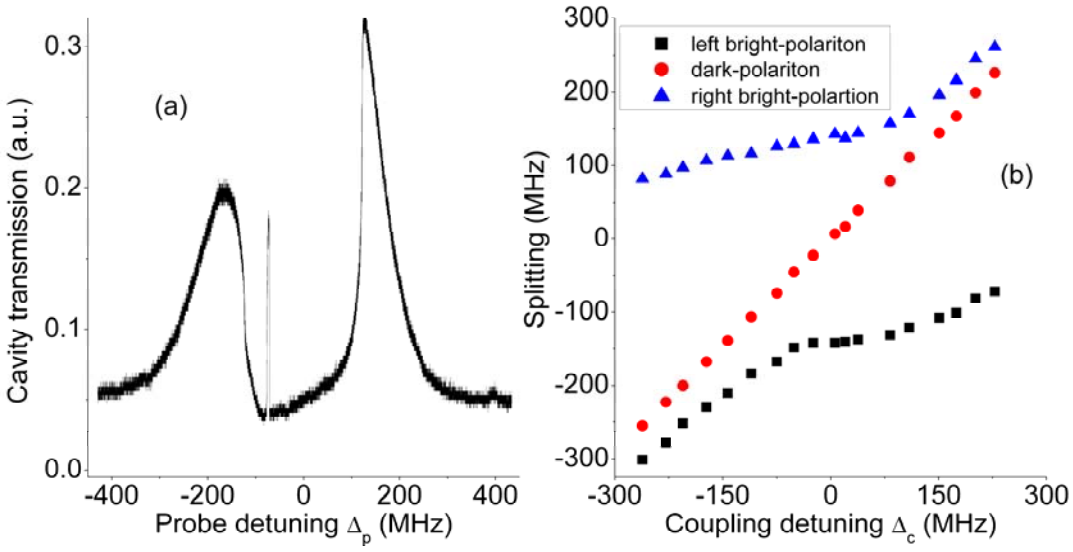

Figure 8, Sheng et al.